Preclinical Development

Molecular Cancer Therapeutics

Preclinical Pharmacology of AZD5363, an Inhibitor of AKT: Pharmacodynamics, Antitumor Activity, and Correlation of Monotherapy Activity with Genetic Background

Barry R. Davies[1], Hannah Greenwood[1], Phillippa Dudley[1], Claire Crafter[1], De-Hua Yu[3], Jingchuan Zhang[3], Jing Li[3], Beirong Gao[3], Qunsheng Ji[3], Juliana Maynard[2], Sally-Ann Ricketts[2], Darren Cross[1], Sabina Cosulich[1], Christine C. Chresta[1], Ken Page[1], James Yates[1], Clare Lane[1], Rebecca Watson[1], Richard Luke[1], Donald Ogilvie[1], and Martin Pass[1]

Abstract

AKT is a key node in the most frequently deregulated signaling network in human cancer. AZD5363, a novel pyrrolopyrimidine-derived compound, inhibited all AKT isoforms with a potency of 10 nmol/L or less and inhibited phosphorylation of AKT substrates in cells with a potency of approximately 0.3 to 0.8 μmol/L. AZD5363 monotherapy inhibited the proliferation of 41 of 182 solid and hematologic tumor cell lines with a potency of 3 μmol/L or less. Cell lines derived from breast cancers showed the highest frequency of sensitivity. There was a significant relationship between the presence of PIK3CA and/or PTEN mutations and sensitivity to AZD5363 and between RAS mutations and resistance. Oral dosing of AZD5363 to nude mice caused dose- and time-dependent reduction of PRAS40, GSK3β, and S6 phosphorylation in BT474c xenografts (PRAS40 phosphorylation $EC_{50} \sim 0.1$ μmol/L total plasma exposure), reversible increases in blood glucose concentrations, and dose-dependent decreases in 2[18F]fluoro-2-deoxy-D-glucose (^{18}F-FDG) uptake in U87-MG xenografts. Chronic oral dosing of AZD5363 caused dose-dependent growth inhibition of xenografts derived from various tumor types, including $HER2^+$ breast cancer models that are resistant to trastuzumab. AZD5363 also significantly enhanced the antitumor activity of docetaxel, lapatinib, and trastuzumab in breast cancer xenografts. It is concluded that AZD5363 is a potent inhibitor of AKT with pharmacodynamic activity *in vivo*, has potential to treat a range of solid and hematologic tumors as monotherapy or a combinatorial agent, and has potential for personalized medicine based on the genetic status of PIK3CA, PTEN, and RAS. AZD5363 is currently in phase I clinical trials. *Mol Cancer Ther; 11(4); 873–87. ©2012 AACR.*

Introduction

The signaling network involving phosphoinositide 3-kinase (PI3K), protein kinase B (PKB, also known as AKT), and mTOR is the most frequently deregulated in human cancer and an important axis for the development of new therapies (1, 2). The network is mutationally activated in distinct ways in different tumor types. For example, in estrogen receptor $(ER)^+$ breast cancers, activating mutations in the catalytic subunit of PI3Kα are common, whereas mutations in AKT1 and PTEN occur at lower frequency (3). In prostate cancer, loss of phosphatases including PTEN and INPP4B are common (4–6). In contrast to the RAF-MEK-ERK pathway, signaling through the PI3K/AKT/mTOR signaling network is noncanonical; the presence of mutations in multiple signaling components in tumor types such as endometrial (7) and bladder (8) supports this concept. PI3K/AKT integrates signaling inputs from many sources including receptor tyrosine kinases and small GTPases, many of which are also commonly amplified or mutated in human cancer, including HER2 and RAS, respectively (9). AKT is a key node in the signaling network, with multiple substrates that mediate processes as diverse as cell proliferation, resistance to apoptosis, and glucose and fatty acid metabolism, which are activated in a wide range of solid and hematologic malignancies (10, 11). AKT activation, either directly or indirectly by loss of PTEN and other means, has been shown to mediate resistance to inhibitors of receptor tyrosine kinases such as HER2 (12, 13), antihormonal agents in breast (14–16) and prostate (17–19) cancers, and chemotherapy (20–22). Therefore, it is one of the most promising targets for cancer therapy, with a considerable platform of preclinical validation.

Authors' Affiliations: [1]Oncology iMED, [2]Imaging, Personalized Healthcare and Biomarkers, AstraZeneca, Cheshire, United Kingdom; and [3]Innovation Center China, AstraZeneca, Shanghai, China

Note: Supplementary material for this article is available at Molecular Cancer Therapeutics Online (http://mct.aacrjournals.org/).

Current address for D. Ogilvie: Paterson Institute for Cancer Research, Wilmslow Road, Manchester M20 4BX, United Kingdom.

Corresponding Author: Barry R. Davies, Oncology iMED, AstraZeneca, Alderley Park, Macclesfield SK0 4TG, UK. Phone: 44-1625-514604; E-mail: Barry.Davies@astrazeneca.com

doi: 10.1158/1535-7163.MCT-11-0824-T

There are a number of ways to inhibit the activity of AKT; 2 distinct types of relatively selective AKT inhibitor are being tested in the clinic. The most advanced agent is MK-2206, an allosteric inhibitor, which binds to the region that interacts with both the pleckstrin homology and kinase domains, and prevents translocation of AKT to the membrane and activation. This compound has been shown to enhance antitumor efficacy by chemotherapeutic agents and molecularly targeted therapies in preclinical models (23) and is currently in phase II clinical trials. The dose-limiting toxicity in the clinic is rash, and modest monotherapy clinical activity has been reported. Classical ATP competitive kinase domain inhibitors, which prevent substrate phosphorylation by AKT, have also been developed. The first of these to be described in detail in the literature was GSK690693 (24). This compound was potent and specific, but lacked oral bioavailability and was withdrawn from development in phase I trials. More recently, compounds with oral bioavailability have been disclosed, from a number of companies including Genentech (GDC-0068), Lilly, and GSK, several of which are in phase I clinical testing. For the development of AZD5363, we were provided with a number of potential starting points arising from our earlier collaboration with Astex Therapeutics and their collaboration with the Institute of Cancer Research, United Kingdom, including the promising chemical series exemplified by the orally active compound CCT129254 (25). Our internal development ultimately led to the identification of the clinical development candidate AZD5363. We now describe the primary pharmacology of AZD5363, a potent pan-AKT kinase inhibitor, with pharmacodynamic properties consistent with the mechanism of action of an AKT inhibitor *in vivo*. AZD5363 inhibits the growth of a range of human tumor xenografts, as monotherapy or in combination with HER2 inhibitors in breast cancer models. AZD5363 also produces very significant tumor regressions in combination with docetaxel in breast cancer xenografts. On the basis of these data, AZD5363 is currently being investigated in phase I clinical trials.

Materials and Methods

Cell culture and reagents

Information on culture conditions, source, and identity testing of cell lines is provided in Supplementary Table S1. The structures of lapatinib and docetaxel are provided in Fig. 1. AZD5363 [(*S*)-4-amino-*N*-[1-(4-chlorophenyl)-3-hydroxypropyl]-1-(7*H*-pyrrolo[2,3-*d*]pyrimidin-4-yl)piperidine-4-carboxamide; structure in Fig. 2A; ref. 26] was prepared as a 10 mmol/L stock solution in dimethyl sulfoxide (DMSO) and stored under nitrogen. The final concentration of DMSO was less than 0.5% in all assays. All antibodies were obtained

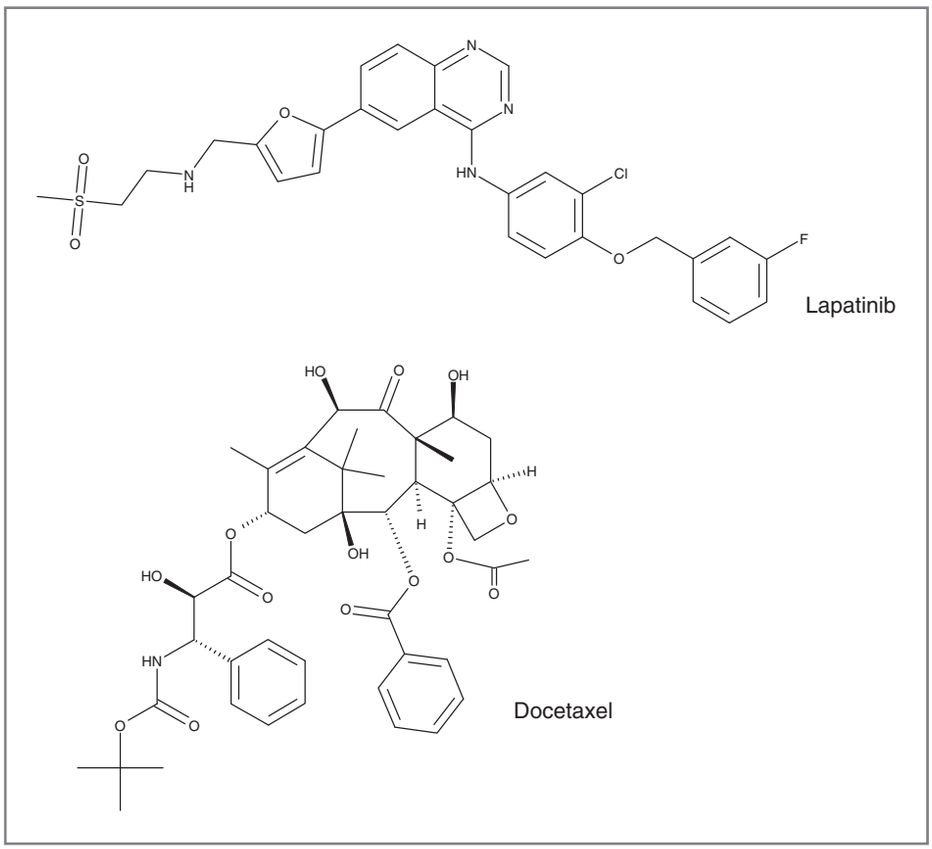

Figure 1. Chemical structures of lapatinib and docetaxel.

from Cell Signaling Technology, except that for PRAS40 (pT246), which was obtained from Biosource.

Enzyme assays

The ability of AZD5363 to inhibit the activity of AKT1, AKT2, and AKT3 was evaluated by the Caliper Off-Chip Incubation Mobility Shift assay. Active recombinant AKT1 (Upstate), AKT2, or AKT3 (both obtained from Invitrogen) were incubated with a 5-FAM–labeled custom-synthesized peptide substrate (Cambridge Research Biochemicals) together with increasing concentrations of inhibitor. Final reactions contained 1 to 3 nmol/L AKT1, AKT2, or AKT3 enzymes; 1.5 μmol/L peptide substrate; ATP at K_m for each AKT isoform; 10 mmol/L $MgCl_2$, 4 mmol/L dithiothreitol (DTT), 100 mmol/L HEPES, and 0.015% Brij-35. The reactions were incubated at room temperature for 1 hour and stopped by the addition of buffer containing 100 mmol/L HEPES, 0.015% Brij-35 solution, 0.1% coating reagent (Caliper), 40 mmol/L EDTA, and 5% DMSO. Plates were then analyzed using a Caliper LC3000, allowing for separation of peptide substrate and phosphorylated product by electrophoresis with subsequent detection and quantification of laser-induced fluorescence. To determine the kinase selectivity profile, AZD5363 was also tested against PKA, ROCK1, ROCK2, and P70S6K. PKA, ROCK1, and ROCK2 activity were determined by Caliper Off-Chip Incubation Mobility Shift Assay, as described earlier. Final reaction conditions for measuring ROCKI activity were 5 nmol/L active recombinant ROCK1 (Invitrogen), 1.5 μmol/L fluorescein isothiocyanate (FITC)-labeled custom peptide substrate, 7 μmol/L ATP, 1 mmol/L DTT, 5 mmol/L $MgCl_2$, 100 mmol/L HEPES, 0.015% Brij-35, and 5 mmol/L β-glycerophosphate; final reaction for measuring ROCK2 activity contained 7.5 nmol/L active recombinant ROCK2 (Upstate), 1.5 μmol/L FAM-labeled custom peptide substrate, 7.5 μmol/L ATP, 1 mmol/L DTT, 10 mmol/L $MgCl_2$, 100 mmol/L HEPES, 0.015% Brij-35, and 5 mmol/L β-glycerophosphate; and protein kinase A (PKA) activity was measured in a final reaction containing 0.0625 nmol/L PKA (Upstate), 3 μmol/L FITC-labeled custom peptide substrate, 4.6 μmol/L ATP, 1 mmol/L DTT, 10 mmol/L $MgCl_2$, 110 mmol/L HEPES, and 0.015% Brij-35. P70S6K activity was measured by a radioactive (^{33}P-ATP) filter-binding assay. Recombinant S6K1 (T412E) was assayed against a substrate peptide (KKRNRTLTV) in a final volume of 25.5 μL containing 8 mmol/L MOPS, 200 μmol/L EDTA, 100 μmol/L substrate peptide, 10 mmol/L magnesium acetate, 20 μmol/L γ-^{33}P-ATP (50–1,000 cpm/pmol), and increasing concentrations of AZD5363. The reactions were incubated for 30 minutes at room temperature and terminated by the addition of 0.5 mol (3%) orthophosphoric acid. Reactions were then harvested onto a P81 UniFilter and product formation quantified. IC_{50} values for all enzyme assays were obtained by fitting data in Origin 7.0. To evaluate a broader selectivity profile, AZD5363 was also tested across the Dundee Kinase Panel at the MRC Protein Phosphorylation Unit, University of Dundee, Angus, United Kingdom.

Cellular inhibition of AKT

A high-throughput screening cell-based assay was developed to measure cellular AKT activity using the MDA-MB-468 breast cancer cell line. Cells were exposed to AZD5363 at concentrations ranging from 3 to 0.003 μmol/L. After a 2-hour treatment, cells were fixed with formaldehyde, washed, permeabilized with 0.5% polysorbate 20 and then probed with a phospho-specific antibody against GSK3β^{ser9}. Levels of phosphorylated GSK3β^{ser9} were measured with an Acumen Explorer laser scanning cytometer (TTP LabTech) and IC_{50} values estimates by fitting data in Origin 7.0.

Western blot analysis

LNCaP prostate cancer cells and BT474c breast adenocarcinoma cells were exposed to AZD5363 at concentrations ranging from 10 to 0.03 μmol/L for 2 or 24 hours. Cells were then lysed on ice with a buffer containing 25 mmol/L Tris-HCl, 3 mmol/L EDTA, 3 mmol/L EGTA, 50 mmol/L NaF, 2 mmol/L sodium orthovanadate, 0.27 mol/L sucrose, 10 mmol/L β-glycerophosphate, 5 mmol/L sodium pyrophosphate, and 0.5% Triton X-100 and protease and phosphatase inhibitors. Lysates were then diluted with sample loading buffer (Invitrogen), separated on 4% to 12% Bis-Tris Novex gels, transferred onto nitrocellulose membranes, and probed with antibodies for phospho-PRAS40, phospho-GSK3β, phospho-S6, phospho-AKT, phospho-4E-BP1, total 4E-BP1, PARP, and caspase-3. After an overnight incubation with the primary antibody, membranes were washed and incubated with horseradish peroxidase-tagged secondary antibodies, followed by visualization of the immunoblotted proteins on a Syngene ChemiGenius with Super-Signal West Dura Chemiluminescence Substrate. Quantification was carried out using Syngene GeneTools, and IC_{50} values were estimated.

FOXO3a translocation assay

BT474c cells were seeded into a clear bottom, black wall 96-well plate, and incubated overnight at 37°C, 5% CO_2 before being exposed to AZD5363 at concentrations ranging from 3 to 0.003 μmol/L. After 2 hours of treatment, cells were fixed with formaldehyde, permeabilized with 0.5% polysorbate 20, and then probed with a primary antibody against FOXO3a overnight at 4°C. Following a wash step, cells were incubated with a secondary antibody conjugated to an Alexa Fluor 488 dye and imaged using a Cellomics ArrayScan. An algorithm measuring the ratio of nuclear to cytoplasmic fluorescence intensity was developed, and IC_{50} values were estimated.

Proliferation assays

Cell proliferation assay was determined by 2 methods, MTS and Sytox Green. Briefly, cells were seeded in 96-well plates (at a density to allow for logarithmic growth during

the 72-hour assay) and incubated overnight at 37°C, 5% CO_2. Cells were then exposed to concentrations of AZD5363 ranging from 30 to 0.003 μmol/L for 72 hours. For the MTS endpoint, cell proliferation was measured by the CellTiter AQueous Non-Radioactive Cell Proliferation Assay (Promega) reagent in accordance with the manufacturer's protocol. Absorbance was measured with a Tecan Ultra instrument. For the Sytox Green endpoint, Sytox Green nucleic acid dye (Invitrogen) diluted in TBS-EDTA buffer was added to cells (final concentration of 0.13 μmol/L) and the number of dead cells detected using an Acumen Explorer. Cells were then permeabilized by the addition of saponin (0.03% final concentration, diluted in TBS-EDTA buffer), incubated overnight and a total cell count measured. Predose measurements were made for both MTS and Sytox Green endpoints, and concentration needed to reduce the growth of treated cells to half that of untreated cells (GI_{50}) values were determined using absorbance readings (MTS) or live cell counts (Sytox Green).

Animals

Specific, pathogen-free, female nude mice (*nu/nu*: Alpk) and male SCID mice (SCID/CB17; 786-0 xenograft studies) were bred at AstraZeneca (Alderley Park) and housed in pathogen-free conditions. Animals were maintained in rooms under controlled conditions of temperature (19°C–23°C), humidity (55% ± 10%), photoperiod (12 hours light/12 hours dark), and air exchange. Animals were housed in standard cages within a flexible film isolator, with food and water provided *ad libitum*. The facilities have been approved by the Home Office License and meet all current regulations and standards of the United Kingdom. The mice were used between the ages of 8 and 12 weeks in accordance with institutional guidelines.

Implantation of cells into mice

For *in vivo* implants, cells were harvested from T225 tissue culture flasks by a 2- to 5-minute treatment with 0.05% trypsin (Invitrogen) in EDTA solution followed by suspension in basic medium and 3 washes in PBS (Invitrogen). Only single-cell suspensions of greater than 90% viability, as determined by trypan blue exclusion, were used for injection. Tumor cells were injected subcutaneously in the left flank of the animal in a volume of 0.1 mL. For BT474c studies the animals were supplemented with 0.36 mg/60-d 17β estradiol pellets (Innovative Research of America) 1 day before cell implantation. For KPL-4 and HGC-27 antitumor studies, tumors were passaged as approximately 10 mm^3 fragments into the flank before carrying out efficacy studies, to achieve more consistent take rates.

Efficacy studies

When mean tumor sizes reached approximately 0.2 cm^3, the mice were randomized into control and treatment groups. The treatment groups received varying dose schedules of AZD5363 solubilized in a 10% DMSO 25% w/v Kleptose HPB (Roquette) buffer by oral gavage, docetaxel (Sanofi-Aventis) solubilized in 2.6% ethanol in injectable water by intravenous injection once on day 1 at 15 or 5 mg/kg once weekly. When administered in combination, docetaxel was administered 1 hour before the oral dose of AZD5363. The control group received the DMSO/Kleptose buffer alone, twice daily by oral gavage. Tumor volumes (measured by caliper), animal body weight, and tumor condition were recorded twice weekly for the duration of the study. Mice were sacrificed by CO_2 euthanasia. The tumor volume was calculated (taking length to be the longest diameter across the tumor and width to be the corresponding perpendicular diameter) using the formula: $(\text{length} \times \text{width}) \times \sqrt{(\text{length} \times \text{width})} \times (\pi/6)$. Growth inhibition from the start of treatment was assessed by comparison of the differences in tumor volume between control and treated groups. Because the variance in mean tumor volume data increases proportionally with volume (and is therefore disproportionate between groups), data were log transformed to remove any size dependency before statistical evaluation. Statistical significance was evaluated using a one-tailed, 2-sample *t* test.

Pharmacodynamic studies

When mean tumor size reached 0.5 cm^3, the mice were randomized into control ($n = 8$ animals) and treatment groups ($n = 5$ animals per group). The treatment groups received 300 or 100 mg/kg acute dose of AZD5363 solubilized in a DMSO/Kleptose buffer, by oral gavage. The control group received the DMSO/Kleptose buffer alone, once by oral gavage. At 2, 4, 8, 16, or 24 hours after dosing, the animals were humanely killed and the tumor was snap frozen in liquid nitrogen and stored at −80°C. Total blood was collected by intracardiac puncture and plasma prepared and immediately frozen at −20°C for pharmacokinetic analysis. Frozen tumors were homogenized using Fastprep methodology lysis matrix A (MP Biomedicals) and lysates generated using adjusted lysis buffer (1% Triton X-100). Equivalent amounts of protein (12 μg per lane) were resolved by 4% to 15% gradient SDS-PAGE premade gels (#345-0035 Bio-Rad) and transferred to nitrocellulose membranes. Membranes were then incubated with primary antibodies tGSK3β (BD Transduction Laboratories #610202), pGSK3β (CST #9336), tS6 (CST #2217), pS6 (CST #2211), and subsequently with HP-conjugated antimouse IgG (CST #7076) or antirabbit IgG (#7074) diluted in 5% marvel in PBS. Immunoreactive proteins were detected by enhanced chemiluminescence (Pierce; #34080) and bands quantified with a ChemiGenius (Syngene). Phosphorylated PRAS40 (T246) was measured by solid phase sandwich ELISA (Biosource #KHO0421)

Radiotracer preparation and positron emission tomography imaging

2[18F]Fluoro-2-deoxy-D-glucose (^{18}F-FDG) was supplied by PETNET solutions. Specific activity was

approximately 185 GBq/mmol. Radiochemical purity (determined by thin-layer chromatography) was greater than 95%. Imaging was carried out using the Inveon positron emission tomography (PET) and computed tomography-docked system from Siemens Medical Solutions. Data were acquired with IAW software (Siemens) Version 1.4.3 and analyzed with IRW software (Siemens) version 3.0. The performance of the scanner has been documented previously (27).

Images were reconstructed using the MAP/3D algorithm (quality control measurement was carried out for the PET scanner before commencement of imaging). Following imaging, tumors were snap frozen in liquid nitrogen and stored at −80°C. Mice received on average 7.96 MBq of radioactivity as a bolus intravenous injection via the tail vein under isoflurane anesthesia. Food was withdrawn on the day of imaging in half-hour intervals so each mouse was fasted for 4 hours before injection of ^{18}F-FDG. Mice were dosed with either vehicle or AZD5363 (130, 200, or 300 mg/kg) and were imaged 4 hours after drug dosing. Mice were anesthetized in preparation for ^{18}F-FDG injection 3 hours and 15 minutes after dosing, and anesthesia was then maintained for a 45-minute uptake period followed by a 20-minute PET scan under isoflurane anesthesia. Anesthesia was induced using isoflurane delivered in 100% oxygen (~1.5% isoflurane, 3 L oxygen). Respiration and temperature were monitored throughout, with body temperature being maintained at 36°C–37°C. Following imaging, tumors were snap frozen in liquid nitrogen and stored at −80°C.

Images were reconstructed using the MAP/3D algorithm (quality control measurement was carried out for the PET scanner before commencement of imaging). Regions of interest (ROI) were manually drawn on the 3-dimensional visualization package of Inveon Research Workplace software, to determine radioactivity uptake in the whole tumor. Data were expressed as the maximum standardized uptake value (SUV). Max SUV was calculated using the following formula described by Gambhir, where ID is the injected dose (28).

$$\text{MaxSUV} = \frac{\text{Maximum radioactivity in ROI (Bq|mm}^3\text{)} \times \text{mouse body weight (g)}}{\text{ID(Bq)}}$$

Blood glucose concentration was measured before vehicle or AZD5363 dosing and after PET scanning. Blood glucose concentrations were measured with an Accu Chek meter (AVIVA, Roche). Data are reported as mean ± SEM unless otherwise stated. Statistical analyses were conducted using GraphPad prism (v. 4.02). An ANOVA allowing for treatment group was carried out as well as group means, which were compared using a 2-sided *t* test.

Plasma pharmacokinetic analyses

Plasma samples were extracted by protein precipitation in methanol. Following centrifugation, the supernatants were mixed with water in a ratio of 1 in 10 (v/v). Extracts were analyzed by high-performance liquid chromatography/mass spectrometry using a reversed phase Gemini column (Phenomenex) and a gradient mobile phase containing water/methanol/formic acid. Peaks were detected using a Micromass/Waters MS technology Ultima mass spectrometer.

Results

AZD5363 is a potent inhibitor of AKT *in vitro*

In isolated enzyme assays, AZD5363 inhibited all 3 isoforms of AKT, with an IC_{50} < 10 nmol/L. P70S6K and PKA were inhibited with similar potency to the AKT isoforms, but a lower potency was shown against the Rho kinases ROCK1 and ROCK2 (Table 1). Further insight into selectivity was obtained by screening the compound at a concentration of 1 μmol/L in a panel of 75 kinases, which included 35 members of the AGC kinase family. AZD5363 had significant activity (>75% inhibition at 1 μmol/L) against 15 kinases, 14 of which were members of the AGC family. These enzymes were AKT1, AKT2, AKT3, P70S6K, PKA, ROCK2, MKK1, MSK1, MSK2, PKCγ, PKGα, PKGβ, PRKX, RSK2, and RSK3 (data not shown).

The activity of AZD5363 in cells was determined by its ability to inhibit phosphorylation of its substrates PRAS40 and GSK3β in BT474c ($Her2^+$ PIK3CA mutant breast) and LNCaP (PTEN-null prostate) cancer cells using Western blotting, and in MDA-MB-468 (PTEN-null breast) cancer cells, by an immunofluorescence-based (Acumen) assay. AZD5363 inhibited phosphorylation of these substrates

Table 1. IC_{50} values of AZD5363 against enzyme and cellular endpoints

Enzyme inhibition n mol/L	
Akt1	3
Akt2	7
Akt3	7
ROCK1	470
ROCK2	60
PKA	7
P70S6K	6
Inhibition of AKT substrates in cells μ mol/L	
pGSK3β	0.76 (BT474c; Western)
	0.06 (LNCaP; Western)
	0.38 (MDA-MB-468; Acumen)
pPRAS40	0.31 (BT474c; Western)
	0.22 (LNCaP; Western)
	0.39 (MDA-MB-468; Acumen)
pFOXO3a translocation	0.69 (BT474c)

NOTE: *In vitro* kinase assays were conducted to determine the potency and selectivity of AZD5363 against Akt1, Akt2, Akt3, and other members of the AGC-kinase family. Cellular assays were used to show cellular potency against AKT substrates.

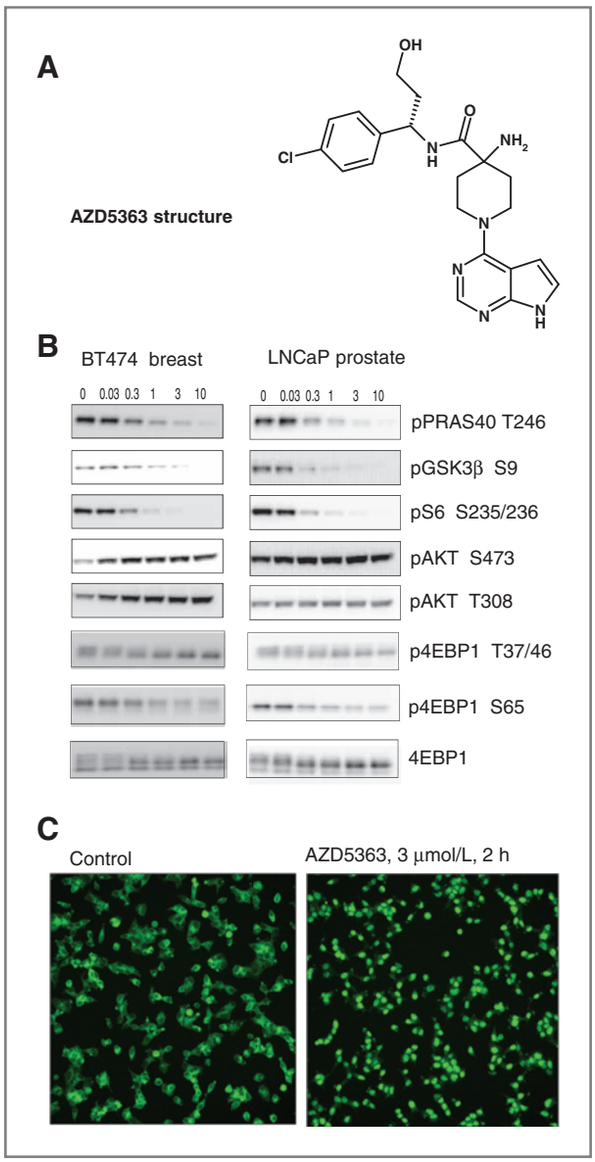

Figure 2. AZD5363 inhibits phosphorylation of AKT substrates and downstream pathway proteins in cells and induces translocation of FOXO3a to the nucleus *in vitro*. A, structure of AZD5363. B, inhibition of cellular AKT substrates in LNCaP and BT474c determined by Western blot analysis of lysates generated following a 2-hour treatment with increasing concentrations of AZD5363. C, induction of nuclear accumulation of FOXO3a in BT474c cells exposed to 3 μmol/L AZD5363 for 2 hours.

with an IC_{50} value of 0.06 to 0.76 μmol/L in the 3 cell lines (Table 1). The phosphorylation status of AKT, and several proteins downstream of AKT in the signaling network, were also monitored by Western blotting in BT474c and LNCaP cells. AZD5363 effectively inhibited phosphorylation of S6 and 4E-BP1 in these cell lines, whereas it increased phosphorylation of AKT at both ser^{473} and thr^{308} (Fig. 2B). The activity of AZD5363 was also measured by its ability to induce nuclear translocation of FOXO3a in BT474c cells. Inhibition of AKT prevents phosphorylation of FOXO3a; this results in translocation of FOXO3a to the nucleus, where it is able to switch on the expression of genes such as p27, FasL, and BIM, which collectively induce cell-cycle arrest and/or apoptosis. In BT474c cells, AZD5363 induced FOXO3a nuclear translocation with a half-maximal effective concentration (EC_{50}) value of 0.69 μmol/L; a concentration of 3 μmol/L was sufficient to almost completely localize FOXO3a to the nucleus (Fig. 2C). To show P70S6K pharmacology of AZD5363 in cells, we used the RT4 bladder cancer cell line. These cells have a homozygous deletion in TSC1 and very low TSC2 expression; hence, AKT is largely uncoupled from P70S6K in these cells. In this cell line, AZD5363 inhibited S6 phosphorylation with an IC_{50} value of approximately 4.8 μmol/L, whereas the allosteric inhibitor MK-2206 was much less active (IC_{50} > 30 μmol/L; Supplementary Fig. S1).

AZD5363 inhibits *in vitro* growth of a subset of tumor cell lines

The activity of monotherapy AZD5363 was measured by its ability to inhibit growth of a panel of 182 cell lines derived from solid and hematologic tumors, by a standard proliferation assay. Tumor cell lines that were inhibited with a $GI_{50} < 3$ μmol/L were classified as sensitive whereas those with a $GI_{50} > 3$ μmol/L were classified as resistant. Forty-one cell lines (23%) were classified as sensitive; 25 of these lines (14%) were inhibited with a $GI_{50} < 1$ μmol/L and were classified as highly sensitive. The highest frequency of sensitivity was seen in cell lines derived from breast cancers (14 of 22; 64%); $HER2^+$ and ER^+ breast cancer cell lines were consistently sensitive (Fig. 3A). Cell lines derived from endometrial, gastric, hematologic, and prostate cancers all showed a frequency of response of 24% to 33%, although only 6 unique prostate cancer cell lines were screened. Cell lines derived from lung and colorectal tumors showed a lower frequency of response at 12% and 7% respectively, whereas all the cell lines derived from bladder cancers were classified as resistant. There appeared to be a correlation between sensitivity to AZD5363 and either the presence of activating PIK3CA mutations, PTEN loss or inactivating mutation, or HER2 amplification. Nineteen of 25 (76%) cell lines classified as highly sensitive and 30 of 41 (73%) the cell lines classified as sensitive carried at least one of these genetic defects (Fig. 3B). When data from the whole-cell panel were analyzed, regardless of other mutations, a significant relationship was found between the presence of PIK3CA mutations and sensitivity to AZD5363 ($P = 0.0059$; t test). When mutations in the helical and catalytic domains of PIK3CA were analyzed separately, a significant correlation was found between both types of mutation and sensitivity to AZD5363 ($P = 0.024$ and 0.0047 for helical and kinase domain mutations, respectively). A significant correlation was also found between PTEN mutation (loss or gene sequence mutation) and sensitivity to AZD5363 ($P = 0.0099$; t test; Supplementary Fig. S2). A significant

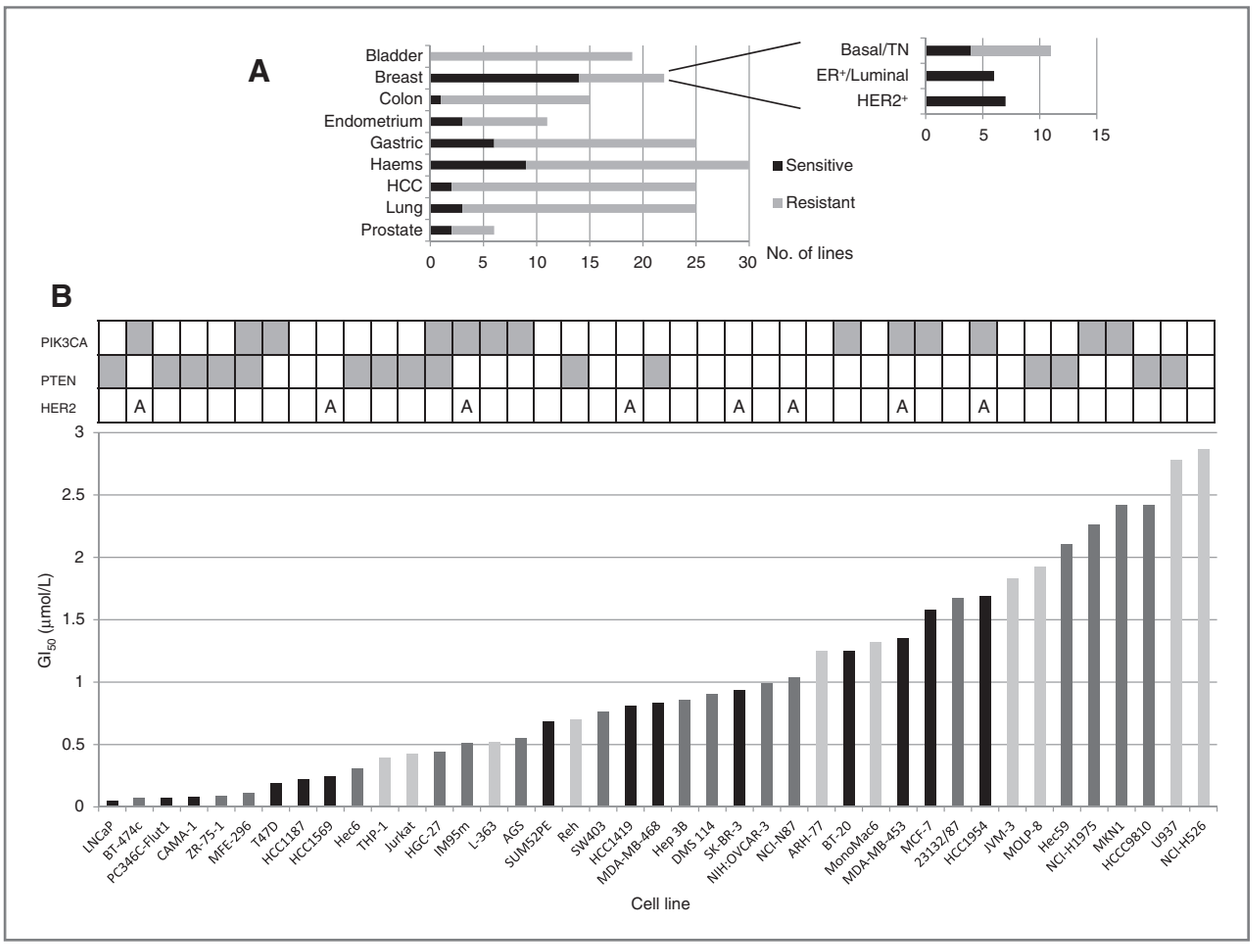

Figure 3. AZD5363 inhibits proliferation of a subset of cancer cell lines *in vitro*. A, panels of cell lines derived from different tumor types were screened in a standard MTS cell proliferation assay. Cell lines with a $GI_{50} < 3$ μmol/L were classified as sensitive, whereas those with a $GI_{50} > 3$ μmol/L were classified as resistant. B, relationship of sensitive ($GI_{50} < 3$μmol/L) and highly sensitive ($GI_{50} < 1$ μmol/L) cell lines with genetic status. The sensitivity of cell lines derived from breast cancers (black bars), other solid tumors (dark gray), or hematologic malignancies (light gray) was related to the presence of mutations in PIK3CA or PTEN or to HER2 amplification (A).

correlation between the presence of a RAS mutation (collectively analyzing K-, N-, or H-RAS mutations) and resistance to AZD5363 was also found ($P = 0.038$; t test). When cell lines with coincident RAS mutations were excluded from the analysis, the relationship between PIK3CA mutation and AZD5363 sensitivity and PTEN mutation and AZD5363 sensitivity was very highly significant ($P < 10^{-5}$ in both cases; Supplementary Fig. S3).

AZD5363 inhibits the growth of human tumor xenografts *in vivo*

The effect of monotherapy AZD5363 on growth of xenografts was determined by continuous oral dosing to nude mice. Dose-dependent inhibition was observed in all models tested. In $HER2^+$ amplified, PIK3CA mutant BT474c xenografts, oral administration at 100 mg/kg twice daily resulted in 80% inhibition ($P < 0.0001$); this schedule was more effective than 200 mg/kg every day (39% inhibition; $P = 0.02$) but less effective than the maximum well-tolerated dose of 200 mg/kg twice daily (104% inhibition; $P < 0.0001$; Fig. 4A). In the $HER2^+$ amplified, PIK3CA mutant HCC-1954 breast cancer xenograft, AZD5363 at 150 mg/kg twice daily caused pronounced tumor regression (129% inhibition; $P < 0.0001$) whereas 75 mg/kg twice daily resulted in 111% inhibition ($P < 0.001$; Fig. 4B). In contrast, 30 mg/kg twice weekly trastuzumab was inactive in this $HER2^+$ model. In 786-0 PTEN-null renal cancer xenografts, AZD5363 at 150 mg/kg twice daily resulted in partial regression (125% inhibition; $P < 0.0001$) whereas 75 mg/kg twice daily caused partial growth inhibition (56%; $P = 0.001$; Fig. 4C). AZD5363 also inhibited growth of PIK3CA mutant/PTEN-null HGC-27 gastric cancer xenografts at doses more than 50 mg/kg twice daily; in this model slight tumor regressions were observed at doses more than 100 mg/kg twice daily, and a dose-dependent time to progression was observed after cessation of dosing (108%, 106%, and 72% inhibition of growth; $P < 0.0001$, 0.001 and

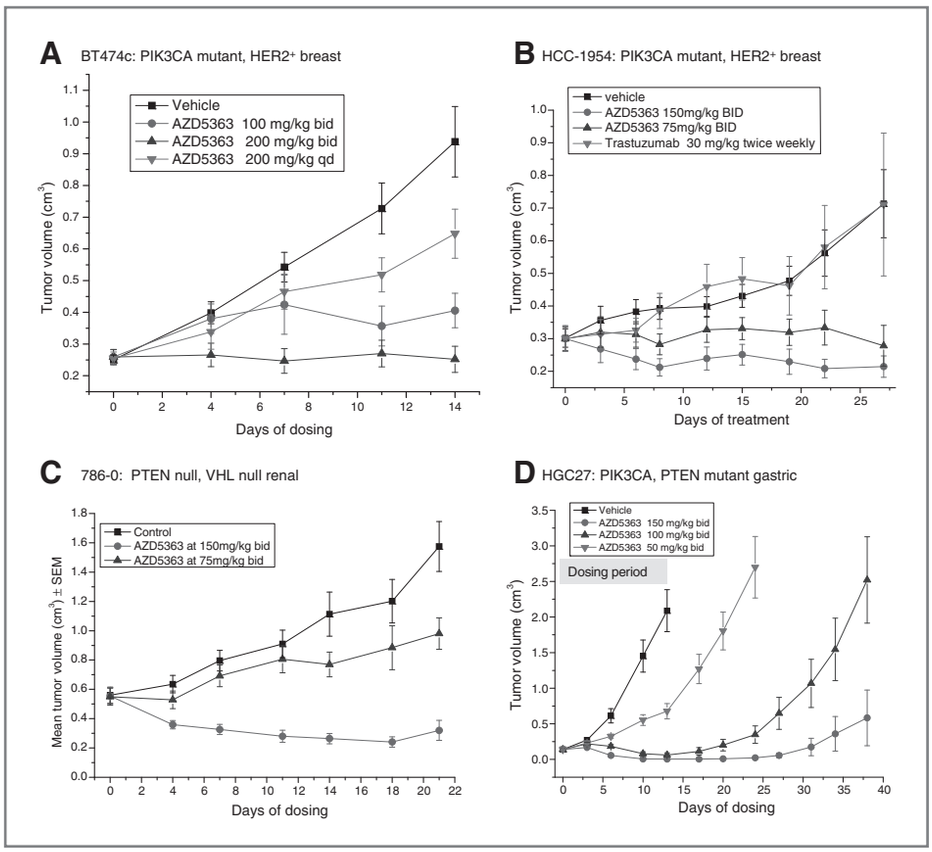

Figure 4. Continuous monotherapy dosing of AZD5363 inhibits growth of xenografts. Xenografts growing in immunodeficient mice were dosed as indicated throughout the experimental period (A–C) or for 16 days before dosing was stopped and recovery of tumor growth monitored (D). qd, daily; bid, twice daily.

0.003 by doses of 150, 100, and 50 mg/kg twice daily respectively; Fig. 4D).

AZD5363 has pharmacodynamic activity *in vivo*

The pharmacodynamic activity of AZD5363 was determined in BT474c xenografts in nude mice, following acute doses of 300 and 100 mg/kg and related to plasma pharmacokinetics (Fig. 5A). Following a 300 mg/kg dose of AZD5363, phosphorylation of PRAS40, GSK3β, and S6 was significantly inhibited for at least 24 hours. pPRAS40 was most strongly inhibited, with approximately 90% inhibition at 1 and 2 hours, and this recovered to approximately 70% inhibition at 24 hours. Inhibition of GSK3β and S6 phosphorylation varied from approximately 80% at 1 hour to approximately 50% at 8 hours and approximately 40% at 24 hours. Total plasma exposure of AZD5363 (not corrected for protein binding) exceeded 10 μmol/L at 1 hour and remained more than 1 μmol/L for approximately 8 hours following a 300 mg/kg dose. Phosphorylation of all 3 biomarkers was significantly inhibited at for at least 8 hours following a 100 mg/kg dose of AZD5363, but the magnitude of inhibition was less than that observed following a 300 mg/kg dose (Fig. 5A). Plasma exposure of AZD5363 was approximately 1 μmol/L for at least 4 hours following a 100 mg/kg dose. Plotting the pharmacodynamic–pharmacokinetic relationship between PRAS40 phosphorylation of individual animals showed that 50% inhibition of pPRAS40 occurred at a total plasma exposure of approximately 0.1 μmol/L AZD5363 (Fig. 5B). A dose- and time-dependent relationship between dose of AZD5363 and blood glucose concentration was also seen in the nonfasted animals used for this study; the glucose concentration increased to approximately 20 mmol/L at 2 hours after a 300 mg/kg dose, and fell back to control levels by 16 hours whereas the glucose concentration increased by less than 2-fold following a 100 mg/kg dose, and fell to control levels by 8 hours (Fig. 5C).

AKT plays a key role in glucose metabolism; its substrates GSK3β and AS160 can modulate glycogen synthesis and glucose transporter function respectively, and signaling through the pathway can regulate glycolytic enzymes including hexokinase and phosphofructokinase. Indeed, AKT activation may, at least in part, explain the Warburg effect—the metabolic shift from oxidative phosphorylation to elevated glycolysis in tumors (29, 30). Therefore, ^{18}F-FDG-PET imaging has potential as a biomarker of pathway output following AKT inhibition. The effect of AZD5363 on ^{18}F-FDG uptake was tested in U87-MG xenografts in fasted nude mice, 4 hours after acute dosing. Doses of 130, 200, and 300 mg/kg AZD5363 all caused a significant decrease in tumor uptake of ^{18}F-FDG compared with vehicle controls, but the blood glucose concentration was only significantly elevated at this time point after 200 and 300 mg/kg doses (Fig. 6A).

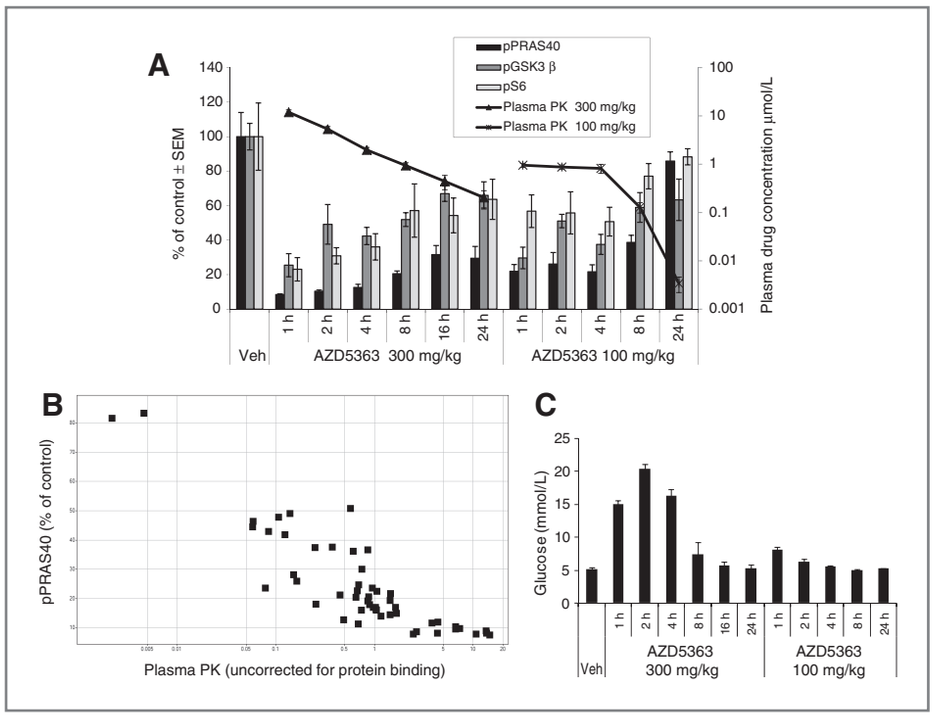

Figure 5. AZD5363 has pharmacodynamic activity in BT474c xenografts and increases blood glucose concentrations in nonfasting nude mice. A, the mean percent inhibition of phosphorylation of GSK3β, PRAS40, and S6 in BT474c ($HER2^+$, PIK3CA mutant) breast cancer xenografts was related to plasma pharmacokinetics (PK). B, relationship between percent inhibition of phosphorylation of PRAS40 and plasma pharmacokinetics of all individual animals. C, relationship of blood glucose concentration with time after acute doses of AZD5363 (nonfasted animals). Veh, vehicle.

Phosphorylation of PRAS40 was also inhibited in the U87-MG xenografts in a dose-dependent manner (Fig. 6B). A dose-dependent effect on tumor growth was also seen after chronic dosing, although this only achieved statistical significance after 7 days dosing at 300 and 200 mg/kg every day; doses of 300, 200, and 130 mg/kg every day, respectively, resulted in 62% ($P < 0.0001$), 36% ($P < 0.001$), and 25% ($P = 0.07$) inhibition of tumor growth (Fig. 6C).

Mechanism of action of AZD5363

To determine whether AZD5363 has a predominantly antiproliferative or proapoptotic mechanism of action, a Sytox Green assay was carried out on a panel of breast and prostate cancer cell lines, which showed sensitivity to AZD5363 in the standard proliferation assay. The Sytox Green assay enables the generation of a dose–response curve based on cell number and determination of percentage of dead cells at a fixed concentration of 1 μmol/L. The GI_{50} values in the Sytox Green assay were generally similar to the proliferation assay values; the values in the 2 assays were all within 5-fold and 8 of 14 (57%) of the cell lines were within 2-fold. However, more than 10% cell death was only seen in 3 of 14 cell lines following incubation with 1 μmol/L AZD5363; these cell lines were BT474c breast and 2 prostate cancer cell lines (LNCaP and PC346C-Flut1; Supplementary Fig. S4A). The induction of cell death was confirmed in the BT474c cell line by exposing the cells to increasing concentrations of AZD5363 and monitoring cleaved caspase-3 and cleaved PARP. A dose proportional increase in both these apoptotic markers was observed in BT474c cells at 48 hours. Given that it seems to be possible to induce cell death in the BT474c cell line *in vitro*, we compared the effects of a continuous and intermittent dosing schedule of AZD5363 that delivered similar areas under curve (AUC) but different C_{max} values on BT474c xenograft growth *in vivo*. Continuous dosing of 100 mg/kg twice daily, which achieved a steady-state exposure of approximately 1 μmol/L AZD5363, resulted in more than 90% inhibition of tumor growth, as shown previously, but no tumor regression (Supplementary Fig. S4B). However, a schedule of 300 mg/kg every 4 days on, 3 days off, which achieves 4-peak concentrations exceeding 10 μmol/L AZD5363, resulted in waves of tumor regression during the dosing period, followed by a recovery of tumor growth in the drug holiday period. When a pharmacodynamic analysis was carried out on these xenografts after short-term chronic dosing (3 days' dosing), there was a significant induction of cleaved caspase-3 at 2 hours following a 300 mg/kg dose of AZD5363, which was not observed after dosing at 100 mg/kg twice daily. In contrast, Ki-67 staining decreased significantly at 8 hours after dosing of both schedules of drug (Supplementary Fig. S4B). These experiments show that a high dose, intermittent schedule of AZD5363 has the potential to be more efficacious than a continuous one in tumors that are susceptible to apoptosis as a consequence of AKT inhibition.

AZD5363 enhances the activity of HER2 inhibitors and docetaxel *in vivo*

The potential of AZD5363 to combine with therapeutic antibodies and small-molecule inhibitors of HER2 signaling was tested in the $HER2^+$, PIK3CA mutant

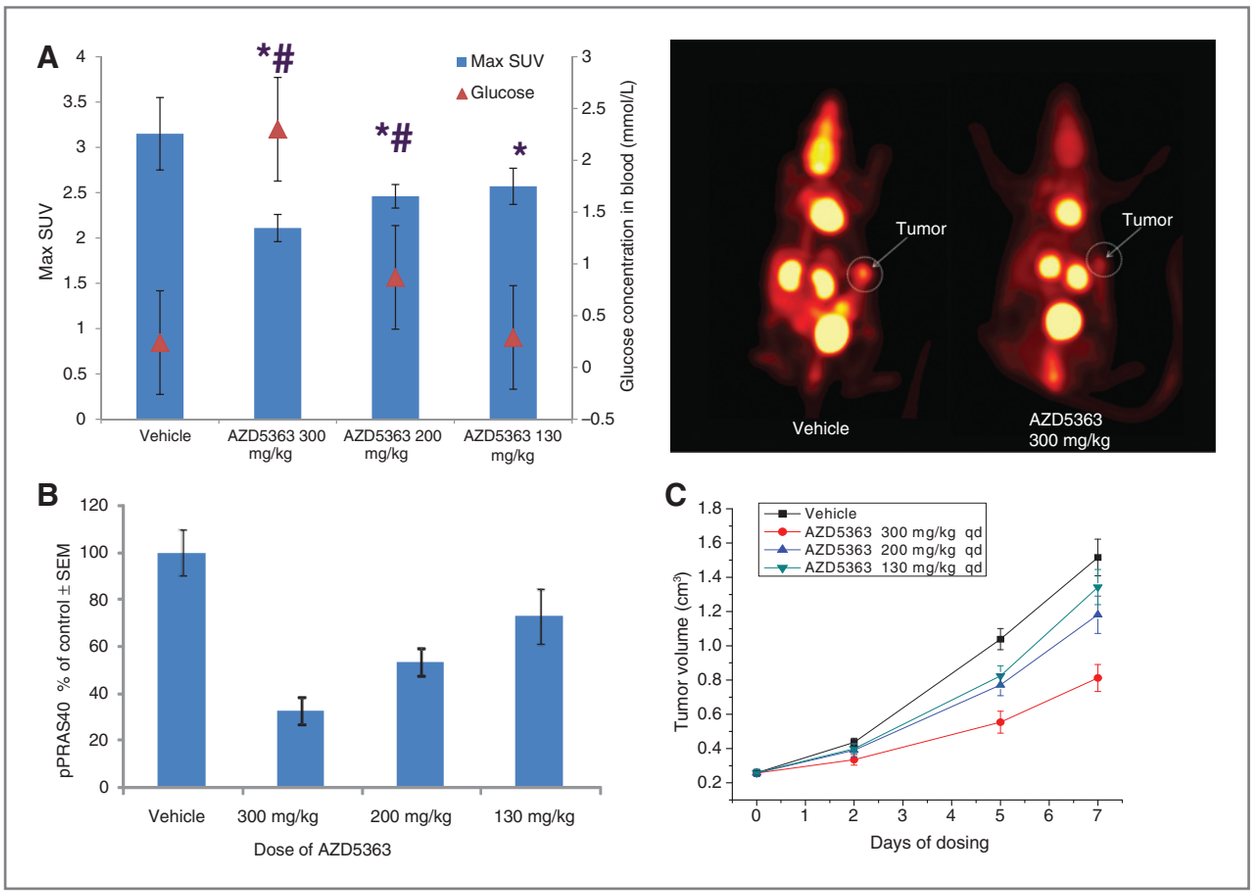

Figure 6. ^{18}F-FDG-PET imaging shows that AZD5363 reduces ^{18}F-FDG uptake in U87-MG xenografts: relationship with tumor pharmacodynamics and growth inhibition *in vivo*. A, tumor ^{18}F-FDG uptake and change in blood glucose concentration following dosing of AZD5363 to fasted animals (mean ± SEM). Vehicle, $n = 9$/group; AZD5363, 130 mg/kg, $n = 10$/group; AZD5363, 200 mg/kg, n = 9/group; AZD5363, 300 mg/kg, $n = 3$/group. Max SUV, *, $P < 0.05$ vs. vehicle; blood glucose, #, $P < 0.05$ vs. vehicle. Representative PET images show change between vehicle and 300 mg/kg AZD5363. B, relationship between inhibition of phosphorylation of PRAS40 at 4 hours and dose of AZD5363 in the imaged xenografts. C, effect of chronic dosing of AZD5363 on the growth of U87-MG xenografts in nude mice. qd, daily.

KPL4 breast cancer xenograft. This model shows suboptimal responses to lapatinib and trastuzumab. Monotherapy lapatinib at 100 mg/kg every day, trastuzumab at 15 mg/kg twice weekly, and AZD5363 150 mg/kg twice daily all inhibited tumor growth (37%, not significant; 69%, $P = 0.002$; and 65%, $P = 0.004$, respectively), but none achieved stasis. In contrast, combinations of AZD5363 and trastuzumab or AZD5363 and lapatinib were well tolerated and, respectively, resulted in tumor regressions of 107% and 109% ($P < 0.0001$). Moreover, the combinations both showed enhanced growth delays after cessation of dosing compared with the monotherapy groups (Fig. 7A). The combination of AZD5363 with docetaxel was tested in 2 different breast cancer xenografts: BT474c and HCC-1187. In BT474c xenografts, a single dose of 15 mg/kg docetaxel resulted in slight tumor regression (129% inhibition; $P < 0.0001$). When combined with 150 mg/kg twice daily of AZD5363, the tumors showed dramatic and greatly enhanced regressions (159% inhibition; $P < 0.0001$), with 6 of 9 tumors showing complete regressions where the tumors were nonmeasurable at the end of the experiment (Fig. 7B). The effect of combining weekly dosing cycles of 5 mg/kg docetaxel with AZD5363 was assessed in the HCC-1187 xenograft model. In the first experiment (Fig. 7C), the combination of 150 mg/kg twice daily of AZD5363 and docetaxel was investigated. The combination was considerably more efficacious than either of the respective monotherapy groups (100% inhibition; $P = 0.0003$ for the combination compared with 71% $P = 0.002$ for monotherapy docetaxel and 79% $P = 0.005$ for monotherapy AZD5363) and showed evidence of increased apoptosis by cleaved caspase-3 staining (Supplementary Fig. S6). In the second experiment (Fig. 7D), the combination of 5 mg/kg once weekly docetaxel with 2 schedules of AZD5363 that deliver equivalent AUCs was investigated. Both schedules enhanced the efficacy of docetaxel monotherapy, and to a similar extent; at the end of the first dosing period docetaxel monotherapy resulted in 76%

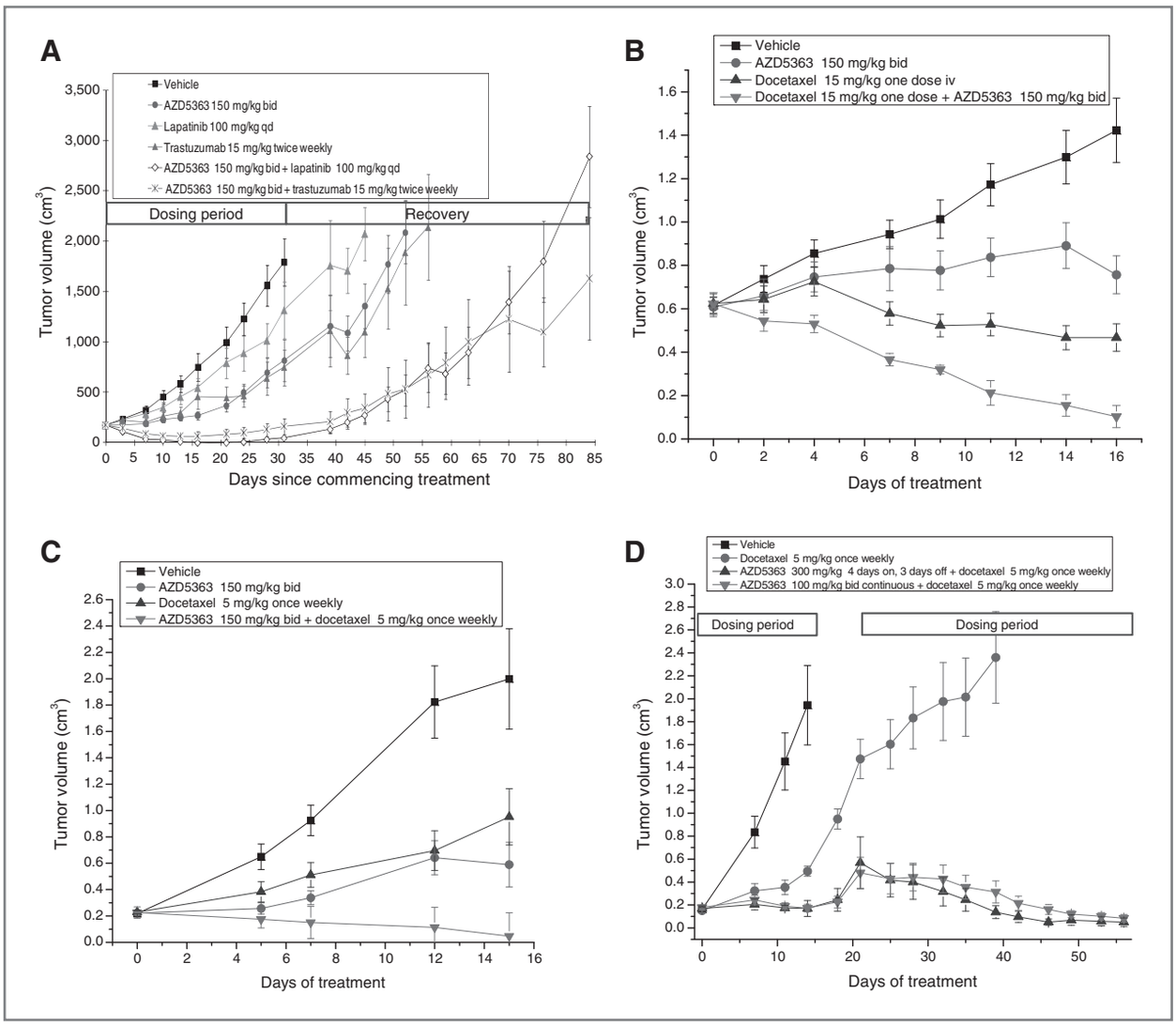

Figure 7. AZD5363 enhances efficacy of trastuzumab, lapatinib, and docetaxel in breast cancer xenograft models. A, combination with trastuzumab and lapatinib in the KPL-4 xenograft. B, combination with docetaxel in the BT474c xenograft. C and D, combinations with docetaxel in the HCC-1187 xenograft. bid, twice daily.

inhibition of tumor growth ($P = 0.0003$) whereas the combinations of docetaxel and the continuous and intermittent dosing schedules of AZD5363, respectively, resulted in 103% and 101% inhibition of tumor growth. All treatment groups showed regrowth when dosing was stopped. Following rechallenge with the same treatments, the docetaxel monotherapy–treated tumors slowly increased in size, whereas the combination groups showed progressive regression. The combination of docetaxel with an intermittent schedule of 300 mg/kg AZD5363 (4 days on, 3 days off) initially appeared to be slightly superior to the combination of docetaxel with a continuous dosing schedule of 100 mg/kg twice daily AZD5363, but the group sizes did not differ significantly from one another at the end of the experiment (Fig. 7D).

Discussion

In our AKT drug discovery program, we ultimately achieved a combination of favorable characteristics relating to potency, selectivity profile, and bioavailability in one small molecule AZD5363. AZD5363 has acceptable preclinical tolerability, pharmacodynamic characteristics of an AKT inhibitor, and a distinct profile from the other AKT inhibitors that have entered clinical development. It is challenging to achieve exquisite selectivity for AGC kinase family members with ATP-competitive AKT kinase inhibitors; AZD5363 is a potent inhibitor of all 3 AKT isoforms, but also carries equipotent pharmacology, at least in enzyme assays, against PKA, P70S6K, and some pharmacologic activity against at least 14 other members of the AGC kinase family. Despite of this additional pharmacology, the profile of activity of AZD5363 in our

182 tumor cell line panel is very similar to that of MK-2206 and GSK690693 (data not shown), suggesting that AKT pharmacology is primarily responsible for its antiproliferative activity. Whereas there is a drop off in potency against AKT substrates in cellular assays compared with AKT enzyme assays, AZD5363 can still inhibit the phosphorylation of at least 2 AKT substrates and induce FOXO3A translocation to the nucleus with a potency of less than 1 μmol/L in sensitive breast and prostate cancer cell lines. AZD5363 also reduces phosphorylation of 4EBP-1, a substrate of mTOR, and increases phosphorylation of AKT itself; this latter phenomenon has been reported to occur with several other ATP competitive, catalytic inhibitors of AKT, and is due to the protein being held in a hyperphosphorylated but catalytically inactive form as a consequence of compound binding (31).

Given that total exposures in excess of 10 μmol/L are achievable at well-tolerated doses in nude mice, it follows that AZD5363 should achieve excellent pharmacodynamic activity *in vivo*. This was indeed found to be the case; AZD5363 inhibited the phosphorylation of PRAS40 and another AKT substrate, GSKβ, and the downstream pathway protein S6 by approximately 80% to 90%, with significant pharmacodynamic activity being maintained for at least 24 hours, following a 300 mg/kg dose to nude mice. Pharmacodynamics showed good correlations with plasma pharmacokinetics; AZD5363 can inhibit the phosphorylation of PRAS40 with plasma EC_{50} value of approximately 0.1 μmol/L in BT474c xenografts growing in nude mice; this is reasonably consistent with an IC_{50} value of approximately 0.3 μmol/L for the same cell line *in vitro*. Therefore, the additional pharmacologic properties of AZD5363 compared with MK-2206 and GSK690693 does not compromise its tolerability and pharmacodynamic activity *in vivo*; in fact the P70S6K pharmacology may be advantageous, resulting in greater inhibition of S6 phosphorylation as a consequence of its direct P70S6K pharmacology in addition to reduced pathway flux as a consequence of AKT inhibition. However, the presence of additional P70S6K pharmacology may also have additional consequences in terms of feedback compared with other AKT inhibitors; P70S6K is known to result in feedback activation of insulin and insulin-like growth factor receptor signaling via IRS1 (32), whereas inhibition of AKT has been reported to remove a feedback loop to these and other receptor tyrosine kinases (33). AKT and P70S6K signaling are known to have an impact on glucose uptake and cellular metabolism, including an upregulation of glycolysis. Therefore, blood glucose concentrations and ^{18}F-FDG-PET imaging have potential as pharmacodynamic, proof-of-principle biomarkers of altered pathway output following inhibition of these kinases. In the nonfasted animals used in the BT474c pharmacodynamic study, a reversible, dose- and time-dependent increase in blood glucose concentration was observed; this was still seen, but attenuated in magnitude, in fasted animals. Similar data have been reported with GSK690693 (34). Moreover, an acute dose of AZD5363 can cause a reduction in ^{18}F-FDG in U87-MG xenografts, using static imaging. This effect correlates with pPRAS40 pharmacodynamics in the same tumor samples, and a dose-dependent reduction in tumor volume following chronic dosing in the same xenograft model. The exact mechanisms by which AZD5363 causes a reduction in ^{18}F-FDG uptake, however, are not fully understood and could be due to various processes; therefore, further experiments are merited using dynamic ^{18}F-FDG-PET to provide information on the metabolic rate of glucose utilization following drug administration.

In contrast to inhibitors with mTOR kinase (35, 36), AZD5363 has much less broad activity in panels of tumor cell lines *in vitro*. Indeed, using a GI_{50} value of 3 μmol/L as a cutoff, only 41 of 182 (23%) of the cell lines were classified as sensitive. Breast cancer cell lines showed the highest frequency of sensitivity, and our data are consistent with previously published data with an allosteric AKT inhibitor, showing that breast cancer cell lines with HER2 amplification and positivity for the ER are sensitive to AKT inhibition (37). Two prostate cancer cell lines with PTEN loss were also particularly sensitive to AZD5363. Luminal breast cancers and prostate cancers have a high frequency of PIK3CA mutation and PTEN loss respectively, whereas having a low frequency of RAS-RAF pathway mutations; moreover HER2 is a strong activator of PI3K-AKT signaling. Therefore, these tumor types appear to be addicted to AKT signaling and are sensitive to monotherapy inhibition by AZD5363. In contrast, cell lines from colon and bladder cancers, which have a high frequency of RAS mutation, are virtually all resistant to AZD5363 monotherapy, even though coincident PIK3CA mutations are present in many of them. Therefore, we sought to determine whether there was a relationship between PIK3CA, PTEN, and RAS mutations, and sensitivity to monotherapy AZD5363, collectively analyzing all the cell lines derived from the various tumor types. The presence of PIK3CA or PTEN mutations significantly correlated with sensitivity to AZD5363, regardless of RAS status, but was very highly significant when coincident RAS mutations were excluded from the analysis; that is, PIK3CA or PTEN mutation/RAS wild-type predicts very highly for sensitivity to AZD5363. The presence of RAS mutation is associated with AKT independence due to redundant activation of cap-dependent translation by convergent regulation of the translational repressor 4E-BP1 by the AKT and extracellular signal-regulated kinase (ERK) pathways (38). It, therefore, follows that tumor types such as breast and prostate cancers may be enriched for responders to an AKT inhibitor such as AZD5363, whereas tumor types with coincident RAS mutations, such as colorectal and endometrial cancers, may require combinations with ERK pathway inhibitors. This having been said, there are mechanisms other than RAS activation that may limit sensitivity to AZD5363. For example, the MCF-7 cell line has a PIK3CA mutation, high P70S6K expression, and wild-type RAS genes, but is considerably less sensitive to AZD5363 growth inhibition ($GI_{50} \sim 1.6$ μmol/L) than the most sensitive breast and prostate

cancer cell lines (GI_{50}s < 0.1 μmol/L); the reason for this comparatively lower sensitivity may be AKT-independent signaling via SGK3 (39). Our findings with AZD5363 are consistent with reports that HER2 amplified and PIK3CA mutant breast cancer cell lines were selectively sensitive and KRAS mutant lines resistant to apoptosis induction by the PI3K/mTOR inhibitor BEZ235 (35, 40). However, PTEN loss of function was associated with resistance to BEZ235 in breast cancer cell lines (40), whereas it is associated with sensitivity to AZD5363 in our cross-tumor cell line panel, suggesting that AKT inhibitors may potentially be more effective in tumors with PTEN loss. This merits further investigation.

The finding that tumor types with either PIK3CA mutation, HER2 amplification, or PTEN loss are particularly sensitive to AZD5363 *in vitro*, logically led us to test the hypothesis that xenografts containing one or a combination of these lesions would be sensitive to AZD5363 monotherapy dosing *in vivo*. Dose-dependent antitumor activity was showed in 4 such models. At the highest doses tested, stasis was observed in a HER2-amplified, PIK3CA mutant breast cancer xenograft, and regressions obtained in another HER2-amplified breast cancer model that was resistant to trastuzumab (HCC-1954), a clear cell renal cancer xenograft with PTEN and VHL loss (786-0), and a gastric cancer model with both PIK3CA mutation and PTEN loss (HGC-27). AZD5363 also greatly enhanced the antitumor activity of trastuzumab and lapatinib in the KPL-4 HER2-amplified breast cancer model, which only showed a modest, progressive disease response to monotherapy doses of these drugs. The data collectively indicate that AZD5363 has the potential to increase response or overcome resistance to HER2-targeting therapies in breast cancer. Other inhibitors of the PI3K/AKT/mTOR network have also been shown to increase the response or overcome resistance to HER2-targeting agents in breast cancer models (41, 42). Interestingly, the HCC-1954 model, which is innately resistant to trastuzumab, expresses high levels of P95HER2, a truncated form of HER2 that lacks the extracellular ligand-binding domain. The presence of this truncated form of HER2 has been reported to correlate with trastuzumab resistance and poor prognosis; however, these tumor types may benefit from treatment with an AKT inhibitor such as AZD5363 (43, 44).

Given that AKT has substrates that can mediate proliferation and resistance to apoptosis, it was surprising to find that AZD5363 monotherapy had an antiproliferative, rather than proapoptotic mechanism of action, at therapeutically relevant doses *in vitro*. Cell death in more than 10% of the cells and biomarkers of apoptosis were only observed in one breast and 2 prostate cancer lines *in vitro*. In the breast cancer cell line where apoptosis was observed *in vitro*, it was possible to achieve waves of apoptosis and tumor regression *in vivo*, by a high, intermittent dosing schedule, whereas an equivalent AUC delivered by a continuous lower dosing schedule was only sufficient to achieve stasis and inhibition of proliferation *in vivo*. AKT is known to mediate resistance to cell death by chemotherapy; we have shown that combination of AZD5363 with docetaxel can result in sustained and profound tumor regression, and by implication, increased apoptosis in 2 breast cancer xenografts. This was achievable with doses of AZD5363 that only cause partial inhibition of tumor growth or stasis as monotherapy. Therefore, the proapoptotic potential of an AKT inhibitor is more likely to be manifested in combination with chemotherapy, than when dosed as a monotherapy. It is possible that the PKA pharmacology of AZD5363 also contributes to the sensitization to apoptosis that we have observed in combination with chemotherapy; inhibiting PKA can decrease RelA phosphorylation that is able to induce cell death in NF-κB expressing, chemoresistant tumor cell lines (45, 46).

In conclusion, AZD5363 is a potent inhibitor of AKT with a pharmacologic profile consistent with its mechanism of action *in vitro* and *in vivo*. Tumor types with PIK3CA mutation, PTEN mutation, or HER2 amplification, without coincident RAS mutation, show the highest frequency of response to AZD5363 *in vitro*; in such tumor types, stasis or regression is achievable by monotherapy dosing *in vivo*. AZD5363 also has potential to overcome resistance or increase sensitivity to HER2 inhibitors in breast cancer, and greatly sensitizes to docetaxel chemotherapy, resulting in tumor regression *in vivo*. AZD5363 is currently in phase I clinical trials.

Disclosure of Potential Conflicts of Interest

B.R. Davies, H. Greenwood, P. Dudley, C. Crafter, D-H. Yu, J. Zhang, J. Li, B. Gao, Q. Ji, J. Maynard, S-A. Ricketts, D. Cross, S. Cosulich, C.C. Chresta, K. Page, J. Yates, C. Lane, R. Watson, R. Luke, and M. Pass are employees of AstraZeneca. D. Ogilvie has ownership interest (including patents) in AstraZeneca. AZD5363 was discovered by AstraZeneca subsequent to a collaboration with Astex Therapeutics (and its collaboration with the Institute of Cancer Research and Cancer Research Technology Limited).

Acknowledgments

The authors thank Holly Ford for her contribution to the development of the FOXO3a translocation assay.

Grant Support

Figure design support was provided by Dr. Zoe van Helmond from Mudskipper Bioscience, funded by AstraZeneca.

The costs of publication of this article were defrayed in part by the payment of page charges. This article must therefore be hereby marked *advertisement* in accordance with 18 U.S.C. Section 1734 solely to indicate this fact.

Received October 14, 2011; revised January 6, 2012; accepted January 20, 2012; published OnlineFirst January 31, 2012.

References

1. Liu P, Cheng H, Roberts TM, Zhao JJ. Targeting the phosphoinositide 3-kinase pathway in cancer. Nat Rev Drug Discov 2009;8:627–44.

2. Hennessy BT, Smith DL, Ram PT, Lu Y, Mills GB. Exploiting the PI3K/AKT pathway for cancer drug discovery. Nat Rev Drug Discov 2005;4:988–1004.

3. Stemke-Hale K, Gonzalez-Angulo AM, Lluch A, Neve RM, Kuo WL, Davies M, et al. An integrative genomic and proteomic analysis of PIK3CA, PTEN, and AKT mutations in breast cancer. Cancer Res 2008;68:6084–91.
4. Cairns P, Okami K, Halachmi S, Halachmi N, Esteller M, Herman JG, et al. Frequent inactivation of PTEN/MMAC1 in primary prostate cancer. Cancer Res 1997;57:4997–5000.
5. Reid AH, Attard G, Ambroisine L, Fisher G, Kovacs G, Brewer D, et al. Molecular characterisation of ERG, ETV1 and PTEN gene loci identifies patients at low and high risk of death from prostate cancer. Br J Cancer 2010;102:678–84.
6. Hodgson MC, Shao LJ, Frolov A, Li R, Peterson LE, Ayala G, et al. Decreased expression and androgen regulation of the tumor suppressor gene INPP4B in prostate cancer. Cancer Res 2011;71:572–82.
7. Cheung LW, Hennessy BT, Li J, Yu S, Myers AP, Djordjevic B, et al. High frequency of PIK3R1 and PIK3R2 mutations in endometrial cancer elucidates a novel mechanism for regulation of PTEN protein stability. Cancer Discov 2011;1:170–85.
8. Platt FM, Hurst CD, Taylor CF, Gregory WM, Harnden P, Knowles MA. Spectrum of phosphatidylinositol 3-kinase pathway gene alterations in bladder cancer. Clin Cancer Res 2009;15:6008–17.
9. Cully M, You H, Levine AJ, Mak TW. Beyond PTEN mutations: the PI3K pathway as an integrator of multiple inputs during tumorigenesis. Nat Rev Cancer 2006;6:184–92.
10. Altomare DA, Testa JR. Perturbations of the AKT signaling pathway in human cancer. Oncogene 2005;24:7455–64.
11. Bellacosa A, Kumar CC, Di Cristofano A, Testa JR. Activation of AKT kinases in cancer: implications for therapeutic targeting. Adv Cancer Res 2005;94:29–86.
12. Nagata Y, Lan KH, Zhou X, Tan M, Esteva FJ, Sahin AA, et al. PTEN activation contributes to tumor inhibition by trastuzumab, and loss of PTEN predicts trastuzumab resistance in patients. Cancer Cell 2004;6:117–27.
13. Berns K, Horlings HM, Hennessy BT, Madiredjo M, Hijmans EM, Beelen K, et al. A functional genetic approach identifies the PI3K pathway as a major determinant of trastuzumab resistance in breast cancer. Cancer Cell 2007;12:395–402.
14. Miller TW, Hennessy BT, Gonzalez-Angulo AM, Fox EM, Mills GB, Chen H, et al. Hyperactivation of phosphatidylinositol-3 kinase promotes escape from hormone dependence in estrogen receptor-positive human breast cancer. J Clin Invest 2010;120:2406–13.
15. Kirkegaard T, Witton CJ, McGlynn LM, Tovey SM, Dunne B, Lyon A, et al. AKT activation predicts outcome in breast cancer patients treated with tamoxifen. J Pathol 2005;207:139–46.
16. Musgrove EA, Sutherland RL. Biological determinants of endocrine resistance in breast cancer. Nat Rev Cancer 2009;9:631–43.
17. Murillo H, Huang H, Schmidt LJ, Smith DI, Tindall DJ. Role of PI3K signaling in survival and progression of LNCaP prostate cancer cells to the androgen refractory state. Endocrinology 2001;142:4795–805.
18. Li B, Sun A, Youn H, Hong Y, Terranova PF, Thrasher JB, et al. Conditional Akt activation promotes androgen-independent progression of prostate cancer. Carcinogenesis 2007;28:572–83.
19. Jiao J, Wang S, Qiao R, Vivanco I, Watson PA, Sawyers CL, et al. Murine cell lines derived from Pten null prostate cancer show the critical role of PTEN in hormone refractory prostate cancer development. Cancer Res 2007;67:6083–91.
20. Wendel HG, de Stanchina E, Fridman JS, Malina A, Ray S, Kogan S, et al. Survival signalling by Akt and eIF4E in oncogenesis and cancer therapy. Nature 2004;428:332–7.
21. Kim D, Dan HC, Park S, Yang L, Liu Q, Kaneko S, et al. AKT/PKB signaling mechanisms in cancer and chemoresistance. Front Biosci 2005;10:975–87.
22. Pei H, Li L, Fridley BL, Jenkins GD, Kalari KR, Lingle W, et al. FKBP51 affects cancer cell response to chemotherapy by negatively regulating Akt. Cancer Cell 2009;16:259–66.
23. Hirai H, Sootome H, Nakatsuru Y, Miyama K, Taguchi S, Tsujioka K, et al. MK-2206, an allosteric Akt inhibitor, enhances antitumor efficacy by standard chemotherapeutic agents or molecular targeted drugs *in vitro* and *in vivo*. Mol Cancer Ther 2010;9:1956–67.
24. Rhodes N, Heerding DA, Duckett DR, Eberwein DJ, Knick VB, Lansing TJ, et al. Characterization of an Akt kinase inhibitor with potent pharmacodynamic and antitumor activity. Cancer Res 2008;68:2366–74.
25. McHardy T, Caldwell JJ, Cheung KM, Hunter LJ, Taylor K, Rowlands M, et al. Discovery of 4-amino-1-(7H-pyrrolo[2,3-d]pyrimidin-4-yl) piperidine-4-carboxamides as selective, orally active inhibitors of protein kinase B (Akt). J Med Chem 2010;53:2239–49.
26. Johnson PD, Leach A, Luke RWA, Matusiak ZS, Morris JJ (inventors); AstraZeneca AB (assignee). Pyrrolo [2, 3-d] pyrimidine derivatives as protein kinase B inhibitors. WO2009/047563. 16th April 2009.
27. Kim JS, Lee JS, Im KC, Kim SJ, Kim SY, Lee DS, et al. Performance measurement of the microPET focus 120 scanner. J Nucl Med 2007;48:1527–35.
28. Gambhir S. Quantitative assay development for PET. InPhelps ME, editor. PET: molecular imaging and its biological applications. Berlin, Germany: Spinger; 2004:130–32.
29. Elstrom RL, Bauer DE, Buzzai M, Karnauskas R, Harris MH, Plas DR, et al. Akt stimulates aerobic glycolysis in cancer cells. Cancer Res 2004;64:3892–9.
30. Garber K. Energy boost: the Warburg effect returns in a new theory of cancer. J Natl Cancer Inst 2004;96:1805–6.
31. Okuzumi T, Fiedler D, Zhang C, Gray DC, Aizenstein B, Hoffman R, et al. Inhibitor hijacking of Akt activation. Nat Chem Biol 2009;5:484–93.
32. Haruta T, Uno T, Kawahara J, Takano A, Egawa K, Sharma PM, et al. A rapamycin-sensitive pathway down-regulates insulin signaling via phosphorylation and proteasomal degradation of insulin receptor substrate-1. Mol Endocrinol 2000;14:783–94.
33. Chandarlapaty S, Sawai A, Scaltriti M, Rodrik-Outmezguine V, Grbovic-Huezo O, Serra V, et al. AKT inhibition relieves feedback suppression of receptor tyrosine kinase expression and activity. Cancer Cell 2011;19:58–71.
34. Crouthamel MC, Kahana JA, Korenchuk S, Zhang SY, Sundaresan G, Eberwein DJ, et al. Mechanism and management of AKT inhibitor-induced hyperglycemia. Clin Cancer Res 2009;15:217–25.
35. Serra V, Markman B, Scaltriti M, Eichhorn PJ, Valero V, Guzman M, et al. NVP-BEZ235, a dual PI3K/mTOR inhibitor, prevents PI3K signaling and inhibits the growth of cancer cells with activating PI3K mutations. Cancer Res 2008;68:8022–30.
36. Yu K, Shi C, Toral-Barza L, Lucas J, Shor B, Kim JE, et al. Beyond rapalog therapy: preclinical pharmacology and antitumor activity of WYE-125132, an ATP-competitive and specific inhibitor of mTORC1 and mTORC2. Cancer Res 2010;70:621–31.
37. She QB, Chandarlapaty S, Ye Q, Lobo J, Haskell KM, Leander KR, et al. Breast tumor cells with PI3K mutation or HER2 amplification are selectively addicted to Akt signaling. PLoS One 2008;3:e3065.
38. She QB, Halilovic E, Ye Q, Zhen W, Shirasawa S, Sasazuki T, et al. 4E-BP1 is a key effector of the oncogenic activation of the AKT and ERK signaling pathways that integrates their function in tumors. Cancer Cell 2010;18:39–51.
39. Vasudevan KM, Barbie DA, Davies MA, Rabinovsky R, McNear CJ, Kim JJ, et al. AKT-independent signaling downstream of oncogenic PIK3CA mutations in human cancer. Cancer Cell 2009;16:21–32
40. Brachmann SM, Hofmann I, Schnell C, Fritsch C, Wee S, Lane H, et al. Specific apoptosis induction by the dual PI3K/mTor inhibitor NVP-BEZ235 in HER2 amplified and PIK3CA mutant breast cancer cells. Proc Natl Acad Sci U S A 2009;106:22299–304.
41. Eichhorn PJ, Gili M, Scaltriti M, Serra V, Guzman M, Nijkamp W, et al. Phosphatidylinositol 3-kinase hyperactivation results in lapatinib resistance that is reversed by the mTOR/phosphatidylinositol 3-kinase inhibitor NVP-BEZ235. Cancer Res 2008;68:9221–30.
42. Junttila TT, Akita RW, Parsons K, Fields C, Lewis Phillips GD, Friedman LS, et al. Ligand-independent HER2/HER3/PI3K complex is disrupted by trastuzumab and is effectively inhibited by the PI3K inhibitor GDC-0941. Cancer Cell 2009;15:429–40.
43. Scaltriti M, Rojo F, Ocana A, Anido J, Guzman M, Cortes J, et al. Expression of p95HER2, a truncated form of the HER2 receptor, and

response to anti-HER2 therapies in breast cancer. J Natl Cancer Inst 2007;99:628–38.

44. Sperinde J, Jin X, Banerjee J, Penuel E, Saha A, Diedrich G, et al. Quantitation of p95HER2 in paraffin sections by using a p95-specific antibody and correlation with outcome in a cohort of trastuzumab-treated breast cancer patients. Clin Cancer Res 2010; 16:4226–35.

45. Manna SK, Manna P, Sarkar A. Inhibition of RelA phosphorylation sensitizes apoptosis in constitutive NF-kappaB-expressing and chemoresistant cells. Cell Death Differ 2007;14:158–70

46. Manna SK, Gangadharan C. Decrease in RelA phosphorylation by inhibiting protein kinase A induces cell death in NF-kappaB-expressing and drug-resistant cells. Mol Immunol 2009;46: 1340–50.